View metadata, citation and similar papers at core.ac.uk
brought to you by CORE
provided by UTHM Institutional Repository

Multi-bifurcation Flow Analysis on 2D Human Respiratory Airway System

Mohd Zamani Ngali
Faculty of Mechanical and Manufacturing Engineering,
Universiti Tun Hussein Onn Malaysia,
86400, Batu Pahat, Johor, Malaysia.
zamani@uthm.edu.my

Kahar Osman Mohd Hazmil Syahidy Abdol Azis
Faculty of Mechanical Engineering,
Universiti Teknologi Malaysia,
81310, Skudai, Johor, Malaysia.
kahar@fkm.utm.my

***Abstract*—Drug inhalation through respiratory airway is the principal method in attaining therapeutic effect for many lung diseases. The multi-bifurcating flow structure acquires deep understanding on the flow driven transportation. This work employs Navier-Stokes equation with Splitting Method numerical flow solver utilizing domain characterization technique. Various breathing conditions are commenced to Weibel's morphometric lung model from fifth to seventh generations of human respiratory system. Velocity distributions, vortex formations and cross-sectional velocity profiles are considered for Reynolds number ranging from resting to moderate exercise breathing. Flow with low Reynolds number retains its symmetric cross-sectional velocity profile across each bifurcation region while higher Reynolds number shows the other way. Drug delivery efficacy is higher with slower inhalation while hard breathing stimulates vortex formations and disturbs drug distributions right through the multi-bifurcation structure.**

Keywords - Multi-bifurcation; Navier-Stokes; Splitting method; drug delivery; respiratory system

I. INTRODUCTION

Non-invasive peroral drug delivery through human airway is used to transport pharmaceutical compounds when there exist symptoms of respiratory diseases. The compounds are expected to evenly reach the end of multi-bifurcating structures where alveoli situated. Wide varieties of breathing techniques were proposed by medical practitioners to optimize the drug delivery efficacy while the flow analyses on the multi-bifurcations are still doubtful.

On the other hand, submerged particle transportation and fluid flow behavior studies has been prolonged and regarded as one of the most prominent field in engineering for centuries. The knowledge is apparently feasible for the great importance of health risk assessments especially on drug delivery formulations. The interdisciplinary efforts have grown greatly during these few decades where computing power has been immensely cultivated. Numbers of notable researches utilizing Computational Fluid Dynamics (CFD) in biomechanics had now came into figure.

While CFD is already an established field by its own, mathematical models, coefficients, correlations, assumptions and numerical experiments related to biomechanics are still in a very progressive phase of maturity before being eminently tied up to the CFD softwares. To date, studies on symmetric multi-bifurcation flow structures [1-4] for instance might not represent an actual respiratory structure but had comparable agreements with experimental and theoretical findings.

Apprehending the importance of understanding the correlations between flow behavior through multi-bifurcations and the drug delivery efficacy, this paper scrutinizes on a clear-cut simulation technique to simulate multi-bifurcation flow and the effect of various breathing conditions on non-invasive peroral drug delivery procedures.

II. NUMERICAL MODELING METHODOLOGY

The process of modeling multi-bifurcation fluid flow starts by constructing the fluid flow solution using an accurate yet efficient numerical solver. Distinct technique is then utilized in order to replicate the numerical domain and discriminate between flows, walls and outer regions. Choices of boundary conditions, initial conditions, assumptions and variables throughout the simulations are emphasized to ensure optimized results.

A. Numerical Fluid Flow Solver

The flow regime in the multi-bifurcation model is developed from the core of momentum equations. The temporal integration of Navier-Stokes equation is achieved using a semi-implicit splitting method, similar to the method of Karniadakis et. al [5] and others. Consider the Navier-Stokes expression below

$$\frac{\partial \vec{v}}{\partial t} + \vec{N}(\vec{v}) = -\nabla p + \frac{1}{R_e}\vec{L}(\vec{v}), \tag{1}$$

where $\vec{L}$ is the linear viscous term and $\vec{N}$ is the non-linear advective term,

$$\vec{L}(\vec{v}) = \nabla^2 \vec{v},$$
$$\vec{N}(\vec{v}) = \vec{v} \cdot \nabla \vec{v}. \tag{2}$$

The continuity equation is imposed at the leading time step,

$$\nabla \cdot \vec{v}^{\,k+1} = 0. \tag{3}$$

In splitting method, (1) is integrated numerically in three for each time step, each stage addressing the three terms independently. Two intermediate velocity fields, $\hat{\vec{v}}$ and $\hat{\hat{\vec{v}}}$, are introduced in order to achieve this. The three stages are,

$$\hat{\vec{v}} - \vec{v}^{\,k} = \left[\frac{3}{2}\vec{N}(\vec{v}^{\,k}) - \frac{1}{2}\vec{N}(\vec{v}^{\,k-1})\right]\Delta t,$$
$$\hat{\hat{\vec{v}}} - \hat{\vec{v}} = -\nabla \bar{p}^{\,k+1}\Delta t,$$
$$\vec{v}^{\,k+1} - \hat{\hat{\vec{v}}} = \frac{1}{2R_e}\left[\nabla^2 \vec{v}^{\,k+1} + \nabla^2 \vec{v}^{\,k}\right]\Delta t. \tag{4}$$

Take divergence of (1) and use the continuity equation to obtain the Poisson's equation for pressure,

$$\nabla^2 \bar{p}^{k+1} = \nabla \cdot \left(\frac{\hat{\vec{v}}}{\Delta t} \right), \tag{5}$$

where the nonlinear term is neglected.

All variables require boundary conditions, including $\vec{v}^{k+1}, \hat{\vec{v}}, \hat{\hat{\vec{v}}}$ and $\bar{p}$. The boundary conditions on $\vec{v}^{k+1}$ are the natural boundary conditions, which must be enforced at the final stage of the splitting method. Boundary conditions on $\hat{\vec{v}}$ and $\hat{\hat{\vec{v}}}$ can be chosen to enhance the numerical aspect of the method. Hence,

$$\hat{\vec{v}} \cdot \vec{k} = \hat{\hat{\vec{v}}} \cdot \vec{k} = 0 \tag{6}$$

on all boundaries.

Finally, there are no natural boundary conditions on the pressure since the value of pressure at the boundary depends on the velocity field in the neighborhood of the boundary. Pressure boundary conditions must be approximated from the governing equations. Take the normal component of (1) to get,

$$\vec{k} \cdot \nabla \bar{p}^{k+1} = \vec{k} \cdot \vec{v}^{k} - \vec{k} \cdot \vec{v}^{k+1} - \vec{k} \cdot \left[\frac{3}{2} \vec{N}(\vec{v}^{k}) - \frac{1}{2} \vec{N}(\vec{v}^{k-1}) \right] \Delta t + \frac{1}{2R_e} \vec{k} \cdot \left[\nabla^2 \vec{v}^{k+1} + \nabla^2 \vec{v}^{k} \right] \Delta t \tag{7}$$

Karniadakis et. al [5] has shown that all the right hand side terms of above equation can be neglected for large Reynolds number, Re, leaving,

$$\vec{n} \cdot \nabla \bar{p}^{k+1} = 0. \tag{8}$$

For that reason, Karniadakis [5] recommends higher order boundary conditions for a better approximation, especially for low Re flow.

B. Numerical Domain Characterizing Technique

This work emphasized on the flow pattern throughout multi-bifurcations of fifth (G5) to seventh (G7) human airway generations, similar to the work by Sheu et al. [6] The geometry construction is known as the Weibel's morphometric lung model [6].

Based on study conducted by Z. Zhang et al. [3] on triple bifurcation flow (G3 to G5), their consideration on lower airway generations is to avoid the turbulent jet effect of the larynx, and to reduce the effect of the cartilaginous rings which appear in the larynx, trachea (G0), and main bronchi (G1). The two-dimensional idealized flow domain is illustrated in Figure 1. The Characteristics of fifth to seventh generation airway are shown in Table I.

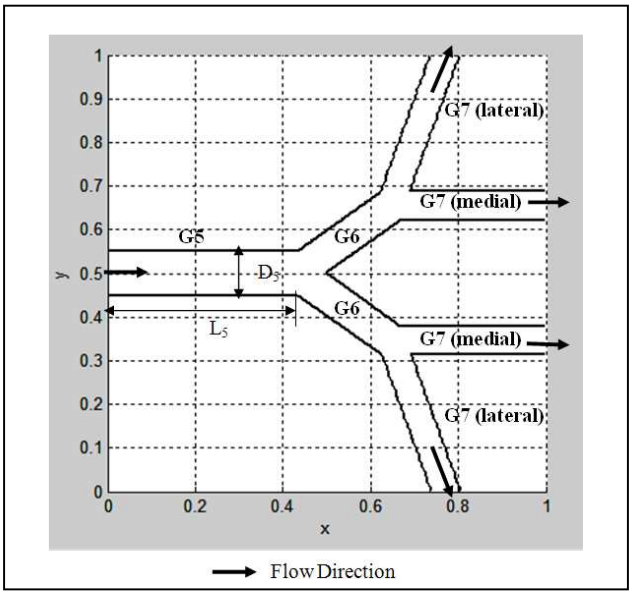

Figure 1. Geometry of the flow domain

TABLE I. CHARACTERISTICS OF FIFTH TO SEVENTH GENERATION AIRWAY

Generation Number z	Number of airways per generation $n(z)$	Airway Diameter D_z (cm)	Airway Length L_z (cm)	Total Cross Section per Generation A(z) (cm^2)
5	32	0.35	1.07	3.11
6	64	0.28	0.90	3.96
7	128	0.23	0.76	5.10

The physical model described was approximated in a two-dimensional finite difference scheme in order to numerically solve the flow problem. The scheme employed grid system of regular Cartesian coordinates. In this system, the grid points are located orthogonal to each other. Finite difference scheme used in this project can only model simple rectangular domain, originally employed to solve lid driven square cavity flow.

Since the physical domain is quite complex, the process in transforming physical boundary into computational boundary could involve quite tedious work; to mathematically develop and integrate new grid transformation algorithm into the original Cartesian finite difference flow solver scheme. Thus, rectangular computational domain was retained with additional implementation of grid point treatment, which classifies the grid points into two categories; normal nodes for grid points those included inside physical flow domain, and null nodes for those fall outside the physical domain.

Every null node located adjacent to the normal nodes but not on the computational boundary is treated as the artificial computational boundary. The advantage of preserving Cartesian grid system and classification of grid points described previously, without implementation of grid

transformation is that, it permits the flexibility on the solution of flow problem in complex domain geometry conveniently. The tasks involved to solve certain flow problem are only in the classifying the nodes and applying boundary conditions.

C. *Numerical Parameter*

The velocities of airflow within human respiratory network are very low and decrease as the flow enters the smaller airways deep down into lungs. For any case, Calay et al. [6] stated that the maximum velocity in human airway corresponds to the Mach number (M) of less than 0.1. Thus in this condition the compressibility can be neglected under the condition that

$$\Delta\rho/\rho_0 = 1/2M^2 \ll 1 .$$

Besides, the air is a Newtonian fluid and dynamic viscosity is independent of the rate of shear. Thus, the airflow can be treated as an incompressible, viscous flow. Under such conditions, the flow is governed by the Navier-Stokes and continuity equations. The relevant air physical properties being considered in this project are 1.225 kg/m^3 density and 1.505 x 10^{-5} m^2/s kinematic viscosity.

In order to capture the flow behavior without temporal variance, steady inhalation flow inside the airway is assumed. Velocity boundary conditions were applied at the inlet of the parent airway (G5) which corresponds to three physical state of inhalation; resting, light activity, and moderate exercise (Zhang et al. [3]), with the inlet flow rate of 15, 30 and 60 l/min into the lung system (i.e through trachea, G0), respectively.

All three breathing conditions and the range of airway generations considered are corresponding Re lower than 2000, thus the flow through the domain can be assumed as laminar and can verify the application of laminar solver to solve the flow problem. Inlet velocities used were parabolic in form (Sheu et al. [6]), assuming developed flow profile from upper airway generation. In this work, the flow problems with inlet Re ranging from 75 to 750 was solved which covered all three states of inhalation.

Besides, outlet velocities were specified at the end of seventh generation airway such that the outlet flow rate are equal between all daughter branches. This is related to the assumption made in the study of Calay [2] that the volume distal to respiratory bronchioles is the same throughout the lungs and the change in volume is the same everywhere.

III. RESULTS AND DISCUSSIONS

Bifurcations along fifth (G5) to seventh (G7) generations of human airways are employed throughout the flow analysis. The passage range is selected as it physically shows sensible display of multi-bifurcation phenomenon with nearly symmetric arrangement and simplicity. This symmetric structure practically permits constructive analysis on the flow pattern that promotes better understanding on each point of discussions.

A. *Velocity distributions for multi-bifurcation flow*

Figure 2 illustrates the flow velocity distributions from G5 to G7 of human airway for three breathing conditions. Flow in G5 shows minimum change in velocity pattern for all resting, light activity and moderate exercise conditions. The flow maintains it flow pattern as shown in both conditions. This is consistent with the laminar flow theory for a straight ductile region fully developed flow pattern.

At the end of the straight region, interesting phenomenon starts when the flow approaches the first bifurcation point. As for all air intake conditions, the flows bifurcate symmetrically to both G6 branches. However, the velocity contours suggest that the flow velocities at the inner walls of G6 branches are higher than those at the outer walls. The gradients are even higher for faster breathing conditions.

With the same length of G6 branches, flow velocity of resting condition travels slower along the passage and recovers to symmetric profile before reaches the second bifurcation points. Meanwhile with higher velocity of the other cases, the momentum of the flows resist the recovery and reach the second bifurcation point with less symmetric profiles. As the bifurcation points between G6 and G7 are at the centre line of G6, the flows bifurcate into G7 branches with different velocity distributions. These significant differences of velocity distributions between G7 branches will lead to less balanced distribution of flow to later generations.

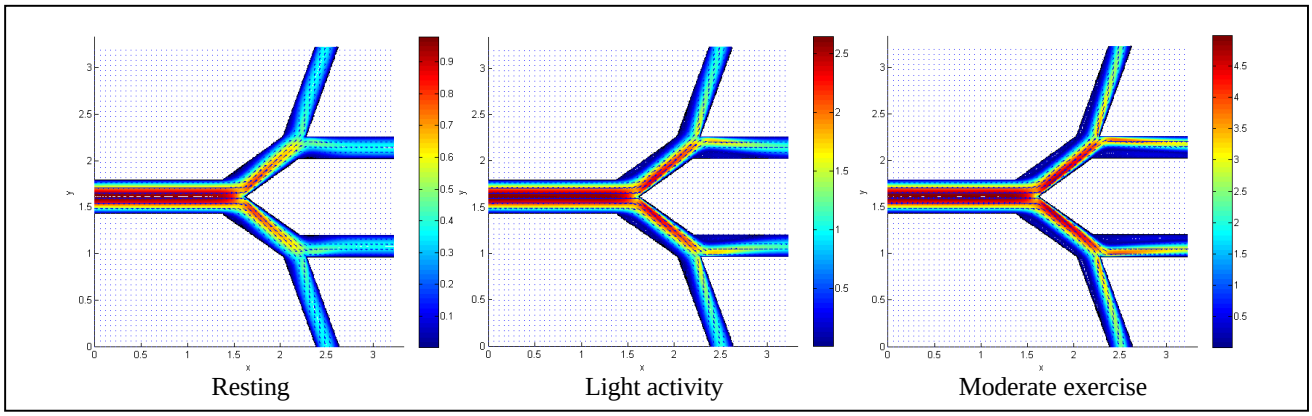

Figure 2. Macro views of flow velocities and streamlines from G5 to G7.

The velocity distributions represented by the contour plots in Figure 2 clearly show that slow breathing as in resting condition is much favorable for more evenly distributed flow through human airway system. On the other hand, air flows tend to distribute in less balanced distribution throughout human airway system for faster breathing conditions. The hypothesis complies with medical advices on drug delivery through breathing where slower breathing is recommended.

B. Vortex formations for various Reynolds number

The presence of vortices in fluid flow plays an important role in the determination of particle deposition flux on fluid walls. Tangential velocity in each vortex is responsible for particles being dragged away from the wall where the vortex located. Figure 3 shows the formations of vortices across the first and second bifurcations for Re ranging from 75 to 350. The stream slices show both the streamlines and the directions of the flow. Any vortex formation is indicated by reversed in flow direction from the main stream trend.

The first vortex appears at the outer wall of G6, just after the corner that separates the G5 and G6 branches. The vortex starts to appear significantly at Re of 150 and continue increasing in width and length as the Re increased to 250. The vortex development shrinks the total area of G6 where the main stream is able to get through. However, the flow figure for Re 350 shows insignificant change in the first vortex width which retains the allowance where the main stream can pass.

While the first vortex starts to appear in lower Re, the second vortex only begin to show up between Re 150 to 250 at the inner wall of G7 medial branch. Although the second vortex appears later, the scale is rather larger and consumes a very good percentage of the total cross-sectional area of G7 medial branch. This condition dramatically reduces the amount of flow area through the acute remaining tolerance. In opposition, the lateral branch of G7 only undergoes a relatively modest vortex for Re as high as 350 due to lower velocity distribution from the forerunner generation. Two significant effects of vortex formations on the flow patterns are observed. The reduction of total cross-sectional area of the flow passage and tendency of vortices drag away any particles that come across are unfavorable for drug delivery effectiveness since it restricts the particles from reaching the affected area.

C. Cross-sectional Velocity profiles for various Re

Figure 4 shows the location of cross sections AA' (G5), BB' (G6), CC' (G7, medial) and DD' (G7, lateral) on the flow domain located at half length of each generation while Figure 5 provides the corresponding plots of normalized axial velocity profile at each of the cross section. From the figure we can observe the effect of increasing Re from resting condition, 150 to moderate exercise, 750.

Normalized velocities are plotted for apparent visualization of the variation of resulting axial velocity profile. Section AA' velocity profiles indicate the same pattern of developed flow for all Re, slight increase in maximum velocity is observed as the Re increases. For Section BB', maximum normalized velocity shifted toward the inner wall side from 0.65D to 0.8D of the flow diameter as Re increases. At Re 350, vortex length is detected to extend to the half length of the G6 airway as reversed flow velocity observed.

Axial velocity profile at Section CC' and DD' provide the flow differences between medial and lateral branches of G7 airways. In medial branches, location of the maximum axial velocity from the inner wall increases from 0.45D (Re 150) to 0.23D (Re 750), closer than in lateral branches with the distances from inner wall ranging from 0.5D to 0.33D, more towards the center of the airway axis. The vortex length extends exceeding half length of the airway at Re more than 450 in medial branch, while there is no vortex extended to the Section DD' for all range of Re considered in lateral branch.

From the axial velocity profile, it is deduced that reversed flow dominate at the first daughter airway G6 and medial (G7) branching after the second bifurcations. Although increasing Re favors the formation of reversed flow in lateral G7 branch, it hardly dominates the said branch even at high Re. The asymmetric flow pattern across the passages for higher Re suggests that such Re does not promote better drug distribution throughout multi-bifurcation structure.

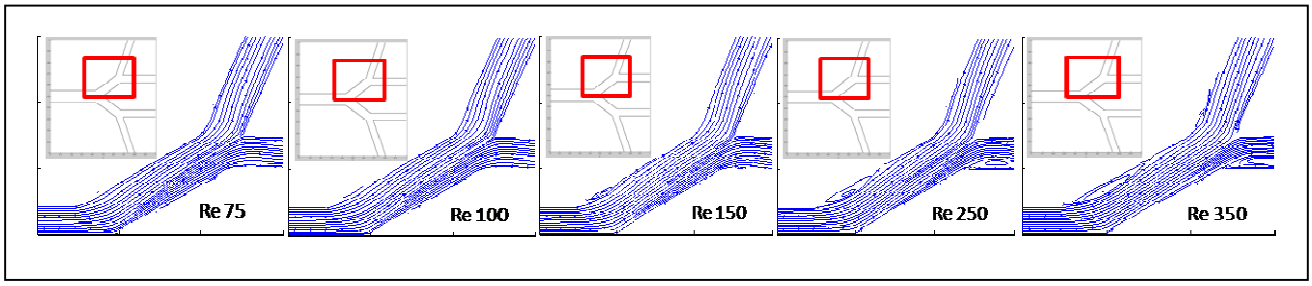

Figure 3. Stream slices for Re ranging from 75 to 350.

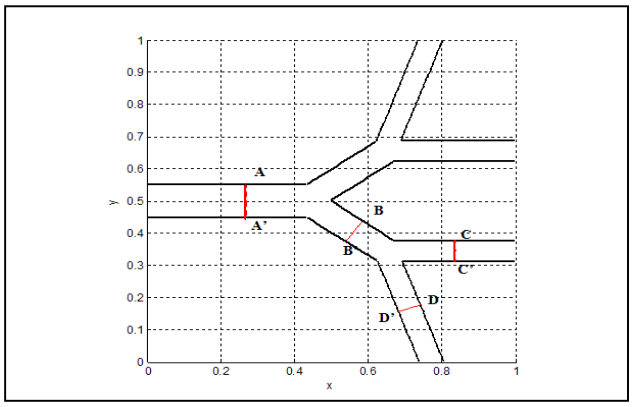

Figure 4. Different cross-section locations for Axial velocity profile; (a) AA' (G5), (b) BB' (G6), (c) CC' (G7, medial), and (d) DD' (G7, lateral)

D. Pressure Distribution

Figure 6 shows the pressure distributions for the three breathing conditions considered in this study. Maximum pressure is identified at the first bifurcation point measured 0.052, 0.325, and 1.15 relative to the initial pressure for case (a), (b), and (c) respectively. High adverse pressure gradient is said to be formed around the carinal region, where the static pressure increases in the direction of flow, leading to a reduced kinetic energy and a deceleration of the developed airflow impinging the bifurcation point and localized region of the inner branch wall close to the bifurcation point.

The hypothesis is supported by velocity distribution in Figure 2, in which high velocity flow in parent tube suddenly become slow i.e. reduce in kinetic energy in the vicinity of the carina. Static pressure is highest at the carinal tip since the center flow stream with high velocity impinges the tip perpendicularly and suddenly stopped. Pressure on the inner wall just downstream reduced since the airstream impinging the wall with lower velocity and at a slanted angle.

As the flow rate of the airstream increases, the magnitude of maximum pressure increases exponentially to account for the sudden conversion of higher kinetic energy to static pressure. The same explanation holds for the formation of the high adverse pressure field around second bifurcation point, except the magnitude is lower as a result of lower airstream entrance velocity into the bifurcation. High adverse pressure field in the first bifurcation point promotes the formation of a localized region of slow-moving fluid stretching away from the wall. This is in conformity with the velocity field at the first bifurcation edge in Figure 2 (a) for the case of resting condition, such that the high velocity region close to the wall just downstream the bifurcation point stretch out from the wall.

After the high pressure region, the pressure becomes uniform. Although the stretch out phenomenon still present, the effect is smaller and it occurs only as a result of viscous force only in order to turn the airflow to a developed flow. For (b) and (c) breathing conditions, the adverse pressure field effect is small because of the high speed airstream. Thus the high velocity region stays closer to the wall after the high pressure field.

Adverse pressure field at the first bifurcation is symmetrical about the parent airway axis. However, it is observed from Figure 5 that this is not necessarily the same case for the second bifurcations. Again, the high pressure field around the bifurcation point of second bifurcations is closely related to the velocity pattern of the entering airstream into the bifurcation region. For resting conditions, the adverse pressure field is symmetric as a result of developed airflow entering the bifurcations.

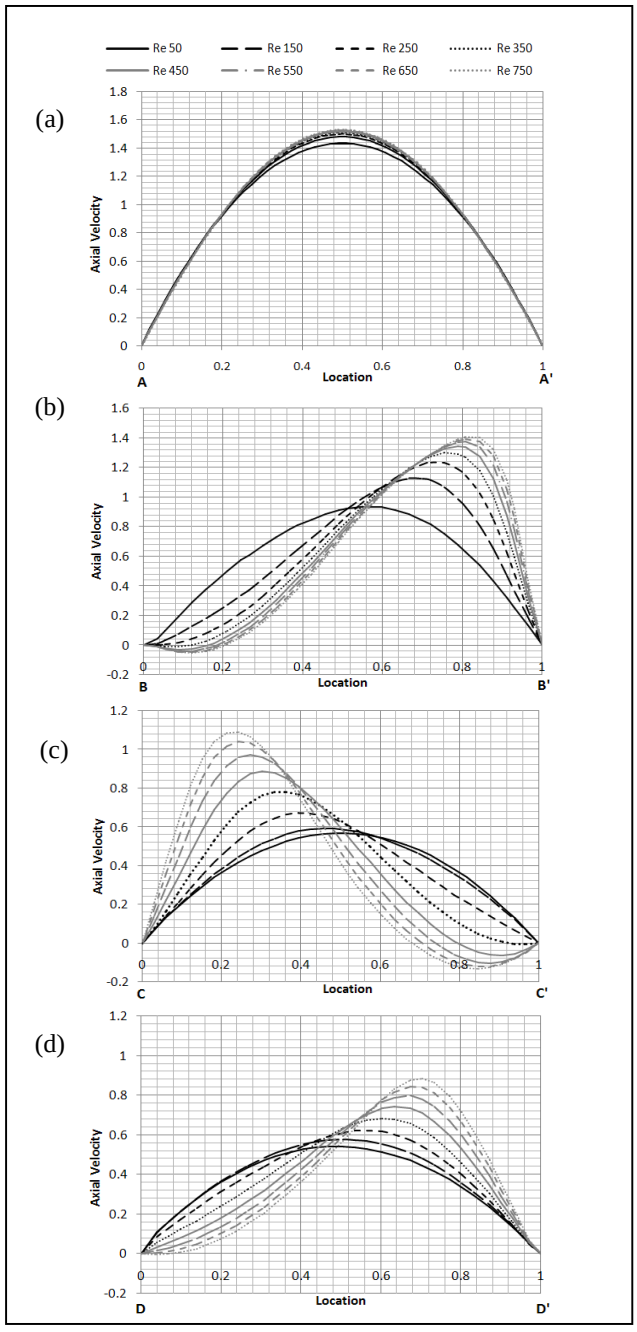

Figure 5. Axial velocity profile at different cross section locations; (a) AA' (G5), (b) BB' (G6), (c) CC' (G7, medial), and (d) DD' (G7, lateral)

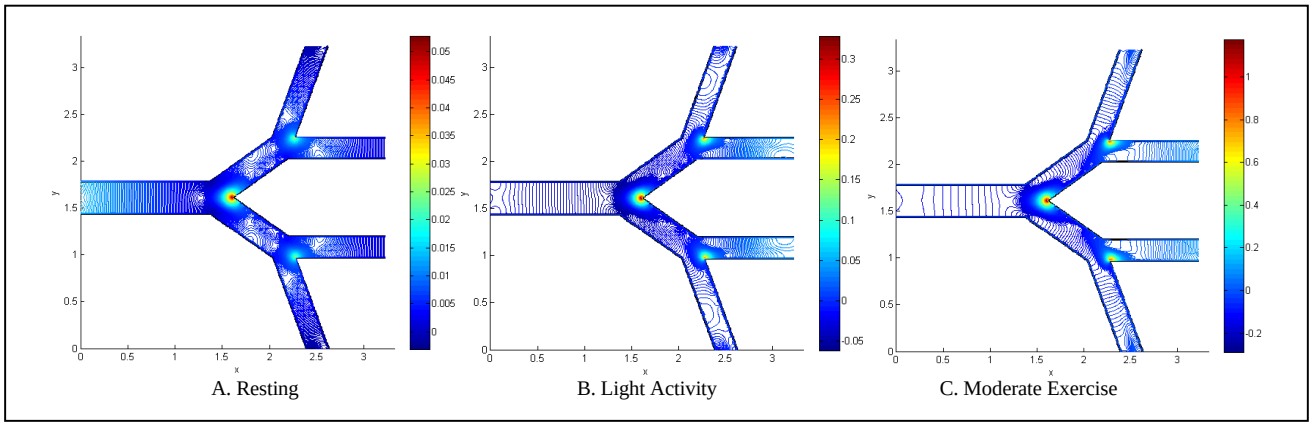

Figure 6. Pressure distribution (normalized) at first bifurcation for all breathing cases

Conversely, adverse pressure field is asymmetrically stretched out into the medial branch as a result of the direction of the entering airstream which is slanted towards lateral branch's axis relative to the axis of the parent airway. For the moderate exercise condition, the adverse pressure field is more stretched out into the medial branch, together with the maximum point of maximum pressure, which is slightly shifted from the carinal tip.

Figure 7 provides another astonishing correlation when the pressure difference between section CC' and DD' of G7 are plotted. At first, there is no significant difference in pressure for low breathing rate. As Re exceeds 175, pressure difference develops and increases exponentially. The asymmetric entrance airstream seems to favor the higher flow rate in the medial branch where lower pressure is observed downstream the lateral branch than those through the medial branch during inhalation. Extending the finding into the actual lower airway flow situation which is transient, it is predicted that alveoli downstream the medial G7 branch would expand prior to the counterparts for high breathing conditions.

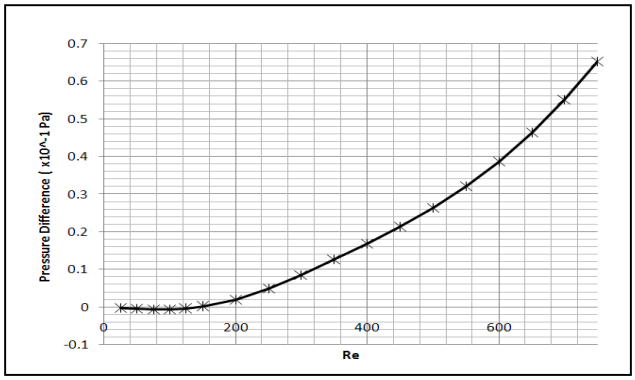

Figure 7. Pressure difference between section CC' and DD'.

IV. CONCLUSION

Numerical flow solver pertaining Navier-Stokes equation with Splitting Method and Domain Characterization Technique was successfully implemented in the multi-bifurcation flow analysis of human respiratory system. Various breathing conditions were commenced to Weibel's morphometric lung model from fifth to seventh generations of the airway system. Velocity distributions, vortex formations and cross-sectional velocity profiles were considered for Reynolds number ranging from resting to moderate exercise breathing. Flow with low Reynolds number retained its symmetric cross-sectional velocity profile across each bifurcation region while flow higher Reynolds number showed the other way. Drug delivery efficacy is expected to be higher with slower inhalation while hard breathing will stimulates vortex formations and disturbs drug distributions right through the airway multi-bifurcation structure.

ACKNOWLEDGMENT

Support and assistance of all members of Computational Fluid Mechanics Laboratory, Universiti Teknologi Malaysia is appreciatively acknowledged.

REFERENCES

[1] C.K. Comer, C. Kleinstreuer, Z. Zhang, "Flow structures and particle deposition patterns in a double-bifurcation airway models". 1. Air flow fields. J Fluid Mech. 435, 25–54, 2001.

[2] R.K. Calay, J. Kurujareon, A.E. Holdo, "Numerical simulation of respiratory flow patterns within human lung". Respiratory Physio. Neurobiology 130, 201-221, 2002.

[3] Z. Zhang and C. Kleinstreuer, "Transient airflow structures and particle transport in a sequentially branching airway model". Phys. Fluids. 14, 862–880, 2002.

[4] Z. Zhang, C. Kleinstreuer, C.S. Kim, "Flow structure and particle transport in a triple bifurcation airway model". J. Fluids Eng. 123, 320–330, 2001.

[5] G. Karniadakis, M. Israeli, and S. Orszag, "High-order splitting methods for the incompressible Navier-Stokes equations," Journal of Computational Physics, 97, pp. 414-443,1991.

[6] T.W.H. Sheu, S.K. Wang, S.F. Tsai, „Finite element analysis of particle motion in steady inspiratory airflow", Comput. Methods Appl. Mech. Engrg. 191, 2681-2698, 2002.